9

Comparison of Granulometric Studies of Brain Slices from Normal and Dissociated Strabismus Subjects Through Morphological Transformations

Jorge D. Mendiola-Santibañez[1], Martín Gallegos-Duarte[2], Domingo J. Gómez-Meléndez[1], Angélica R. Jiménez-Sánchez[3] and Israel M. Santillán-Méndez[1]

[1]*División de Investigación y Posgrado de la Facultad de Ingeniería, Universidad Autónoma de Querétaro, Centro Universitario S/N, CP. 76010, Querétaro*

[2]*Posgrado de la Facultad de Medicina, Departamento de Investigación, Universidad Autónoma de Querétaro, Clavel # 200, Fraccionamiento Prados de la Capilla, Santiago de Querétaro*

[3]*Universidad Politécnica de Querétaro, Carretera Estatal 420 S/N, El Rosario, El Marqués, CP. 76240 Querétaro México*

1. Introduction

Notation

μ, λ scalars (i.e. positive numbers)

B structuring element

$\check{B}$ transposed of the structuring element B, i.e., $\check{B}= \{-x : x \in B\}$

$\wedge$ inf operator

$\vee$ sup operator

Z^+ integer and positive numbers space

$f(x), g(x)$ numerical function of x

$\varepsilon_\mu(f)(x)$ morphological erosion size μ

$\delta_\mu(f)(x)$ morphological dilation size μ

$\gamma_\mu(f)(x)$ morphological opening size μ

$\varphi_\mu(f)(x)$ morphological closing size μ

$\tilde{\gamma}_\mu(f)(x)$ opening by reconstruction size μ

$\tilde{\varphi}_\mu(f)(x)$ closing by reconstruction size μ

$(\psi_\lambda)_{\lambda \in Z^+}$ a family of transformations depending on an unique positive parameter λ

χ_{WM} normalized volumetric measure of granulometric residues of clear structures conforming the image

ζ_{GM} normalized volumetric measure of granulometric residues of dark structures conforming the image

CS Control subject

SS subjects with dissociated strabismus

$SSAV$ Strabismus syndrome of angular variability

WM , GM white and grey matter, respectively.

DHD Dissociated horizontal deviation

$SSAV1$, $SSAV2$ subject 1 and subject 2 with strabismus syndrome of angular variability

$DHD1$, $DHD2$ subject 1 and subject 2 with dissociated horizontal deviation

DBM Digitized brain mapping

CT Computed tomography

Occipital lobe is located in the posterior portion of brain, contiguous to parietal and temporal lobes. Brain lobes present at their most superficial portions, pyramidal as well as starred neurons forming nuclei conforming GM. These neurons are ordered in six laminae on the brain surface to form the brain cortex. The cellular groups in this cortical regions are disposed in an orderly fashion forming columns; their axons extend deeper into the WM (1).

WM is composed by neuronal axons interconnecting cortical zones with other nuclei, for example, magnocellular (great size) and parvocellular (small size) cells, whose projections go to the geniculate lateral bodies toward the cerebral cortex of the occipital lobes (1).

GM, as well as WM, are part of the visual pathway, but only the most superficial layer of the brain that contains cellular nuclei conforming the GM is known as brain cortex; whereas the WM is basically constituted by the axons of these cells (2)(3).

The cerebral cortex is traversed by circumvolutions (gyrus and sulcus) of varied aspects, making it difficult to identify with precision where a brain specific cortical area begins and ends, when it is first observed by means of conventional neuroimaging studies, as is the case of MRI or computed tomography (CT) (1)(2)(3). In spite of this difficulty, it has been possible to obtain important advances in cerebral cortex morphometric studies by means of voxel-based morphometry (VBM). In (4), the authors find a GM diminution in the calcarine sulcus containing the primary visual cortex; they also demonstrate reductions in parieto-occipital areas and in the ventral temporal cortex in children and adult patients with amblyopia. This condition is characterized by dimness of vision with no-improvement in spite of using the best optical correction. In the same way, but using a MR-based morphometric technique, a study on adult patients with exotropia (5), reports a GM increase in motor cortical regions, in conjunction with a diminution in visual cortex, suggesting morphometric changes related to cerebral plasticity. In spite of these morphometric advances, no studies are available in which alterations in the WM and GM in child cerebral cortex with congenital strabismus are compared with that of healthy children of the same age.

On the other hand, congenital strabismus affects 3% of the world-wide population. Nevertheless, it is not known with precision, the anatomical site or microstructural damage underlying the origin of the disease and the zones or nuclei involved. This situation arises from the difficulty of applying morphometric studies in vivo, which would provide an accurate identification of the involved zones and nuclei and would give a better description of diseases such as dissociated strabismus, which is a form of congenital strabismus (6)(7)(8). Therefore, evidence related to the etiology of this disease has been collected from neurofunctional studies (6)(7)(8)(9).

Some forms of dissociated strabismus, besides presenting alterations in the digitized brain mapping (DBM), show ocular movements with angles of variable presentation. When movement is directed in ward, the condition is called SSAV, when it is directed outward it is known as DHD. This last visual alteration is generally symmetrical and concomitant with posterior electroencephalographic alterations, while SSAV tends to present more anterior and asymmetric alterations (6)(7)(8)(9).

Cortical areas in dissociated strabismus can be observed and differentiated with high accuracy by means of techniques of optical dissector as those employed in (10). These authors show, in rodents, changes in cortical cellular density related to visual activity using optical dissector techniques or in vitro methods such as cytochrome oxidase (11)(12)(13). As a result of these studies, the authors demonstrate the presence of structural changes in monkey's cerebral cortex with strabismus and amblyopia; however, given the nature of these methods, it is not possible to apply them to strabismic children.

Up to the present moment, no morphological alterations have been described in any of the varieties of strabismus. But based on the experience drawn from neurofunctional studies of patients with dissociated strabismus, using DBM (6)(7)(8), single photon emission computerized tomography (SPECT) (14)(15) and nuclear proton magnetic resonance spectroscopy (H-NMRS) (9) it is expected that forthcoming evidence on this subject will soon allow the identification of microstructural changes.

Moreover, for the first time, by means of DBM (7)(8), the participation of the cerebral cortex in dissociated strabismus was demostrated. This finding was lately verified by means of SPECT studies. This technique enabled the localization of cortical areas involved in dissociated strabismus and in an epilepsy case. SPECT results (14)(15) showed neuroadaptive changes consistent with the improvement of glucose consumption in the cerebral cortex of patients with strabismus treated with the botulinic toxin or surgery.

The combined application of DBM and H-NMRS methods has demonstrated that cortical regions in dissociated strabismus patients present neuroelectric and biochemical alterations compatible with epileptogenous disease (9). The difficulty lies in identifying, by means of neuroimage studies applied to live subjects, the microstructural alterations related to the origin of dissociated strabismus in children; these micro-alterations cannot be determined with conventional methods of imagenology such as CT or MRI. So far, one alternative for identifying structural changes in cortical regions would be by means of a granulometric analysis of the diverse regions under study.

Granulometric analysis is a methodology developed within mathematical morphology. Mathematical morphology is a technique widely used in image processing. This technique

was initially used to solve a real problem applied to the study of porous means in materials science (16). Currently, one of its multiple applications is the processing of medical images.

In this paper we present a methodology to segment brain MRI [1] by using the morphological opening by reconstruction (17; 18). In particular, the segmentation of regions included in the occipital lobe and areas nearest to this brain structure is performed. Subsequently, two granulometric studies are carried out in a similar way to that followed in granulometric density studies (19). The first study, consists in analyzing clear and dark structures in the segmented deskulling brain for SS and CS groups. Subsequently, a similar procedure is done but on the WM and GM for the subject under study. In each of the granulometric studies, mean patterns are obtained and compared against the granulometric patterns belonging to the CS group. This comparison enables the establishment of volumetric differences, and the introduction of an index, which is useful to understand the behavior of the structures detected in the WM and GM for CS and SS.

It is important to mention not only that the age of the six participants in this study is seven years old; but also that, the GM and WM are segmented by using the methodology followed in (20). From the latter procedure, only some output images are presented to illustrate such segmentations.

This paper is organized as follows. In section 2, a background of the different transformations and concepts related to mathematical morphology are presented. The morphological opening and closing are defined in subsection 2.1. While the opening and closing by reconstruction are presented in subsection 2.2. In subsection 2.3, the granulometry notion, as well as the equations that work in a way similar to those in granulometric density are given. On the other hand, a methodology to segment regions of interest from MRI by using morphological transformations is provided in section 3. In subsection 3.1 several patterns describing the granulometric density of clear structures, dark regions, WM and GM are introduced. The intervals considered for the different structure sizes and a volumetric analysis based on a given index are reported in section 4. Finally, conclusions are presented in section 5.

2. Background on morphological transformations

As follows a background on morphological transformations employed for the treatment of MRIs is presented.

2.1 Definitions of some morphological transformations

In mathematical morphology increasing and idempotent transformations are frequently used. Morphological transformations fulfilling these properties are known as morphological filters (16; 21; 22). The basic morphological filters are the morphological opening $\gamma_{\mu B}(f)(x)$ and closing $\varphi_{\mu B}(f)(x)$ using a given structural element. In this paper, a square structuring element is employed, where B represents the structuring element of size 3×3 pixels, which contains its origin. While $\check{B}$ is the transposed set ($\check{B}= \{-x : x \in B\}$) and μ is a homothetic parameter.

[1] The MRIs used in this paper were obtained from an equipment Philips Intera of 1.5 T (Philips Medical Systems Best Netherlands), using a sequence fast feel echo (FFE), with echo time TE = 6.9 ms, repetition time TR = 25 ms, deviation angle FA = 30 degrees, excitation number NSA = 1, vision field FOV = 230 mm and slice number = 120.

Formally, the morphological opening $\gamma_{\mu B}(f)(x)$ and closing $\varphi_{\mu B}(f)(x)$ are expressed as follows:

$$\gamma_{\mu B}(f)(x) = \delta_{\mu \check{B}}(\varepsilon_{\mu B}(f))(x) \quad and \quad \varphi_{\mu B}(f)(x) = \varepsilon_{\mu \check{B}}(\delta_{\mu B}(f))(x) \tag{1}$$

where the morphological erosion $\varepsilon_{\mu B}(f)(x)$ and the morphological dilation $\delta_{\mu B}(f)(x)$ are $\varepsilon_{\mu B}(f)(x) = \wedge\{f(y) : y \in \mu\check{B}_x\}$ and $\delta_{\mu B}(f)(x) = \vee\{f(y) : y \in \mu\check{B}_x\}$. Here, $\wedge$ is the inf operator and $\vee$ is the sup operator.

The morphological opening and closing can be interpreted in the following way, both morphological transformations allow the elimination of components that can not be contained by the structuring element. Morphological opening works in the interior of the function, while the morphological closing in the complement of the function.

On the other hand, throughout the paper, we will use size 1, or size μ of the structuring element. Size 1 means a square of 3×3 pixels, while size μ means a square of $(2\mu + 1)(2\mu + 1)$ pixels. For example, if the structuring element is size 3, then the square will be 7×7 pixels, i.e, 49 neighbors are analyzed. In any size of the structuring element the origin is located at its center.

In Fig.1 the erosion, dilation, opening and closing are illustrated by using a size 5 structuring element.

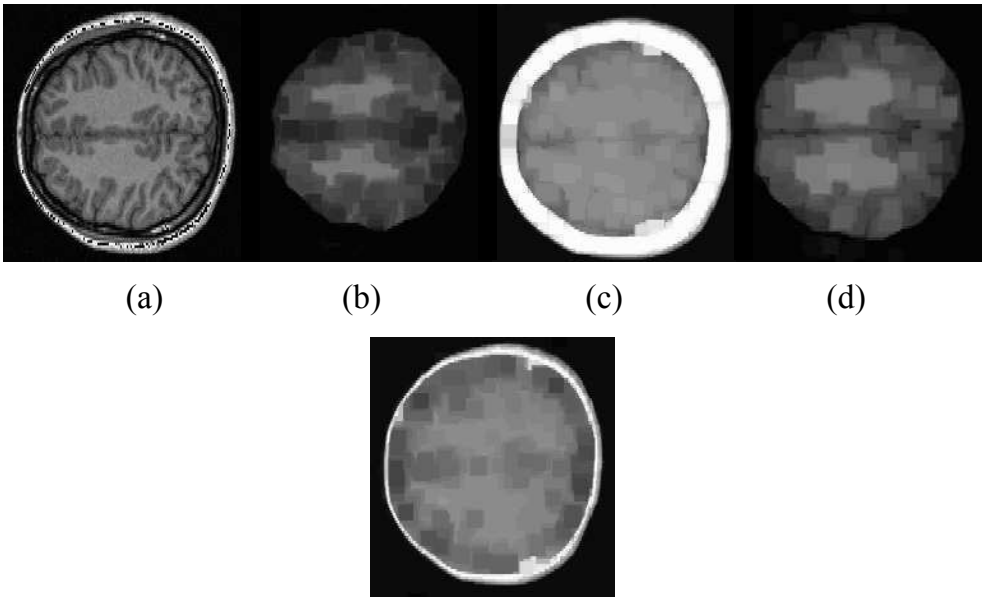

Fig. 1. Images illustrating several morphological operators using a structuring element size 5. a) Input image, b) erosion, c) dilation, d) opening, and e) closing.

2.2 Opening and closing by reconstruction

The reconstruction transformation notion is a useful concept introduced by mathematical morphology. These transformations allow the elimination of undesirable regions without considerably affecting the remaining structures of the image. This characteristic is due to the fact that these transformations are built by means of geodesic transformations (19). The geodesic dilation $\delta_f^1(g)(x)$ and the geodesic erosion $\varepsilon_f^1(g)(x)$ of size one are given by $\delta_f^1(g)(x)=f(x) \wedge \delta(g)(x)$ with $g(x) \leq f(x)$ and $\varepsilon_f^1(g)(x)=f(x) \vee \varepsilon(g)(x)$ with $g(x) \geq f(x)$, respectively. When the function $g(x)$ is equal to the erosion or the dilation of the original function, we obtain the opening $\tilde{\gamma}_{\mu B}(f)(x)$ and the closing $\tilde{\varphi}_{\mu B}(f)(x)$ by reconstruction (17; 18; 23):

$$\tilde{\gamma}_{\mu B}(f)(x) = \lim_{n\to\infty} \delta_f^n(\varepsilon_{\mu B}(f))(x) \quad and \quad \tilde{\varphi}_{\mu B}(f)(x) = \lim_{n\to\infty} \varepsilon_f^n(\delta_{\mu B}(f))(x) \tag{2}$$

In Fig. 2 the performance of the opening and closing by reconstruction is illustrated. Note in Figs. 2(c) and 2(d) that some components have been eliminated, while the remaining are maintained equal to those in the original image.

2.3 Granulometry

Granulometry is the distribution by sizes of particles that constitute an aggregate; it is employed in diverse areas to describe the qualities of size and shape of individual grains within a product. The concept of granulometry was introduced by G. Matheron at the end of the sixties and is presented as follows (24).

Definition 1 (Granulometry)**.** *Let $(\psi_{\lambda\geq 0})_{\lambda\in Z^+}$ be a family of transformations depending on an unique positive parameter λ. This family constitutes a granulometry if and only if the next three properties are verified: (i) $\forall$ positive λ, ψ_λ is increasing; (ii) $\forall$ positive λ, ψ_λ is antiextensive, and (iii) $\forall$ positive λ and μ, $\psi_\lambda\psi_\mu = \psi_\mu\psi_\lambda = \psi_{max(\lambda,\mu)}$*

The family of morphological openings and closings for the numerical case $\{\gamma_{\mu B}\}$, $\{\varphi_{\mu B}\}$ with $\mu = \{1, .., n\}$ fulfils this last definition.

In this paper, we try to detect some characteristics of the different structures conforming the image by means of plots; which are obtained in a way similar to a granulometric density (19). Equations 3 and 4 are used in this article to deduce the granulometric plots. Such equations enable us to obtain a normalized volumetric measure of the granulometric residues of clear (χ_{Clear}) and dark (ζ_{Dark}) structures conforming the image (25; 26). Note that the structures of different dimensions are detected from the diverse μ sizes of the structuring element.

$$\chi_{Clear} = \frac{vol(\gamma_{(\mu-1)B}(f)(x)) - vol(\gamma_{\mu B}(f)(x))}{vol(f(x)) + 1} \tag{3}$$

$$\zeta_{Dark} = \frac{vol(\varphi_{\mu B}(f)(x)) - vol(\varphi_{(\mu-1)B}(f)(x))}{vol(f(x)) + 1} \tag{4}$$

Where *vol* represents the volume; the unit has been added in the denominator of equations 3 and 4 to avoid any indetermination.

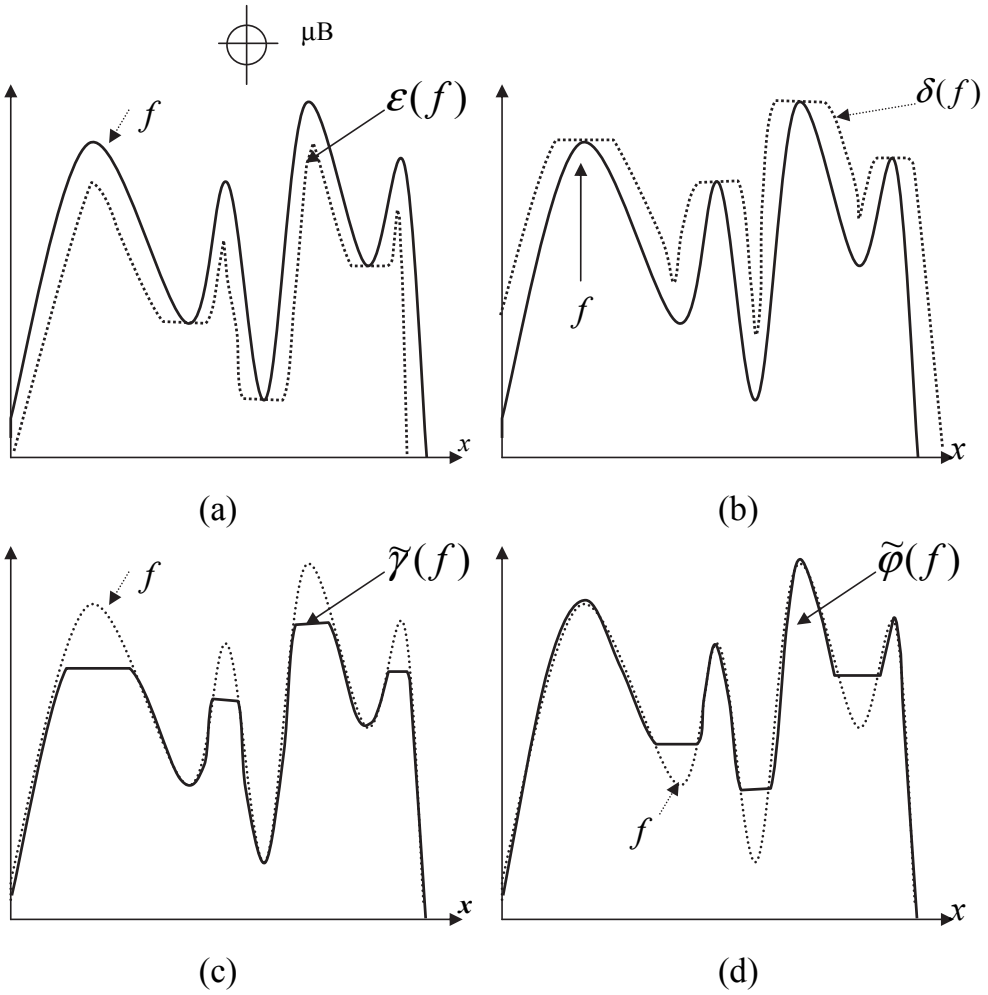

Fig. 2. a) Original image f and the marker $g = \varepsilon(f)$, b) Original image f and the marker $g = \delta(f)$, c) Opening by reconstruction, which uses erosion as marker, d) Closing by reconstruction, which uses dilation as marker.

In Fig. 3 the procedure to find χ_{Clear} on one slice is illustrated; this procedure is the same in the case of equation 4. On the other hand, in the last image of Fig. 3, the arithmetic difference is calculated between openings of sizes 5 and 6. This last image illustrates well some components that are not visible at first sight; however, they are detected by a granulometric process.

3. MRI processing through morphological transformations

In Fig. 4 we present a set of brain MRI slices belonging to a patient with dissociated strabismus classified as SSAV (in the following, in order to simplify the notation we will use for example,

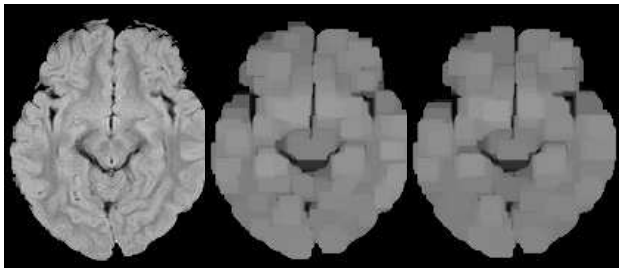

$vol(f) = 16393$ pixels

$vol(\gamma_{\mu=5}) = 16138$ pixels

$vol(\gamma_{\mu=6}) = 16094$ pixels

$\chi_{Clear} = 0.00268$

$\gamma_{\mu=5} - \gamma_{\mu=6}$

Fig. 3. Exemplification of the procedure followed to obtain the χ_{Clear} value of one slice. Bottom image illustrates the arithmetic difference between openings.

the acronym SSAV1 to denote subject 1 with dissociated strabismus classified as SSAV; and the same is extended for DHD subjects.)

The interest in analyzing the regions nearest and within the occipital lobe comes from the finding that in patients with dissociated strabismus, using DBM, an important increment in the electrical activity in the alpha rhythm has been observed (7; 8; 14; 15). This rhythm has been associated with an occipital distribution. An example of these maps is provided in Fig. 5, in which we can note, in black color, an increment in the electrical activity in the alpha rhythm, in accordance with the scale situated at the right and top of the images. In this way, ten axial slices are considered for analysis. The slices are parallel and within the visual via.

On the other hand, images in Fig. 4 are useful to present examples of output images, after the algorithm to carry out the deskulling step is applied.

As follows, we introduce the algorithm to achieve the deskulling step for the regions under study. This algorithm was applied to images acquired from the subjects in this study (CS and SS).

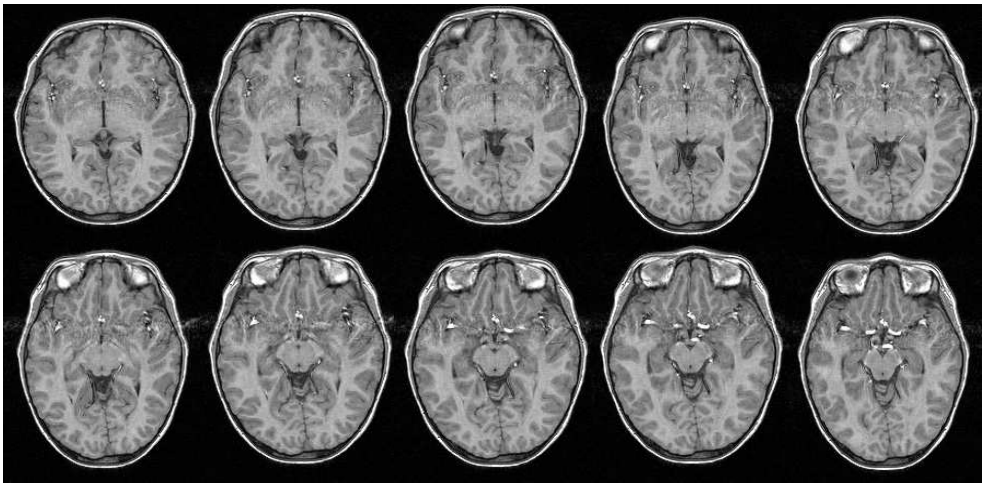

Fig. 4. High resolution axial slices taken from SSAV1

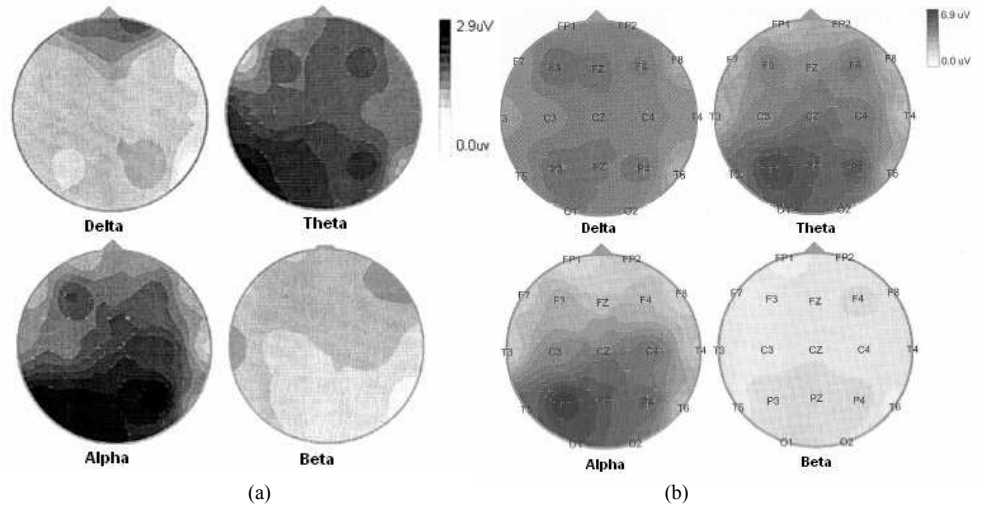

Fig. 5. DBMs showing the electrical behavior of two strabismic children. Darker regions indicate greater electrical activity. (a) Subject with DHD, (b) Subject with SSAV.

Algorithm (deskulling step):

i) Given that the interest zones are located around and within the occipital lobe, the original images located in Fig. 4 are cropped at section 160 to separate the regions of interest. This is illustrated in Fig. 6(a).

ii) Once the images are cropped, we proceed to the deskulling step. For this, the opening by reconstruction size 6 is employed (see equation (2)). The opening by reconstruction has the property of avoiding the generation of new structures. In Fig. 6(b), a set of output images is presented.

iii) Thresholding of the images in Fig. 6(b) between sections 80-255. Here the skull is eliminated and several pores appear in the binary image as a result of the thresholding procedure. The processed images are shown in Fig. 6(c).

iv) Subsequently, a closing by reconstruction size 6 is applied with the purpose of closing the pores originated by the thresholding. The output images are displayed in Fig. 6(d).

v) A mask is obtained with respect to the original image (see Fig. 4), i.e. every pixel in the images in Fig. 6(d) takes the corresponding grey level in the original image. This situation is presented in Fig. 6(e).

vi) A manual segmentation is carried out by a specialist in strabismus. Several undesired regions in the images of Fig. 6(e) are eliminated. The suppressed regions correspond mainly to dura mater and cerebellum; this can be appreciated in Fig. 6(f).

With respect to step ii) of the mentioned algorithm, an opening by reconstruction size 6 is applied. This size was elected from the graphic in Fig. 7(a). The plot was obtained by computing the volume on the image $\widetilde{\gamma}_{\mu} - \widetilde{\gamma}_{\mu+1}$. Such graphic shows the contained structures (clear regions) in the image of size μ. Observe that an important structure of white regions is found between values 1-3, where the skull information is located. To verify this, in Fig. 7(b) we have the original image, on the right we have the eroded image size 3; and this eroded image is used as marker to obtain the opening by reconstruction (last image on the right). However, given that the skull is surrounded by regions with lower intensity levels, a marker given by the morphological erosion of size $\mu = 6$ does not allow the skull reconstruction with its original intensity levels. In Fig. 7(c), the erosion size 6 for several input images is presented; these images are used as markers to obtain the opening by reconstruction. If smaller sizes of the structuring element are selected, for example $\mu = 1$, then the skull is not completely attenuated and the proposed algorithm fails in step iii). For this reason it is crucial to have this situation in mind . In Fig. 8 we illustrate the application of the opening by reconstruction size $\mu = 1$ to the images located in Fig. 6(a). Note that pixel intensity levels in the skull are hardly attenuated.

3.1 Granulometric patterns

Once the skull has been separated and the undesirable regions on the images have been suppressed, a granulometric study is carried out to determine the χ_{Clear} and ζ_{Dark} values on the segmented slices. χ_{Clear} and ζ_{Dark} quantities(see equations 3 and 4) provide information about the distribution density of the clear and dark structures within the image. In Fig. 9 we present in a general way the procedure to obtain the granulometric patterns for dark regions for both CS cases, and one SS. A similar method is applied in the case of clear structures. In

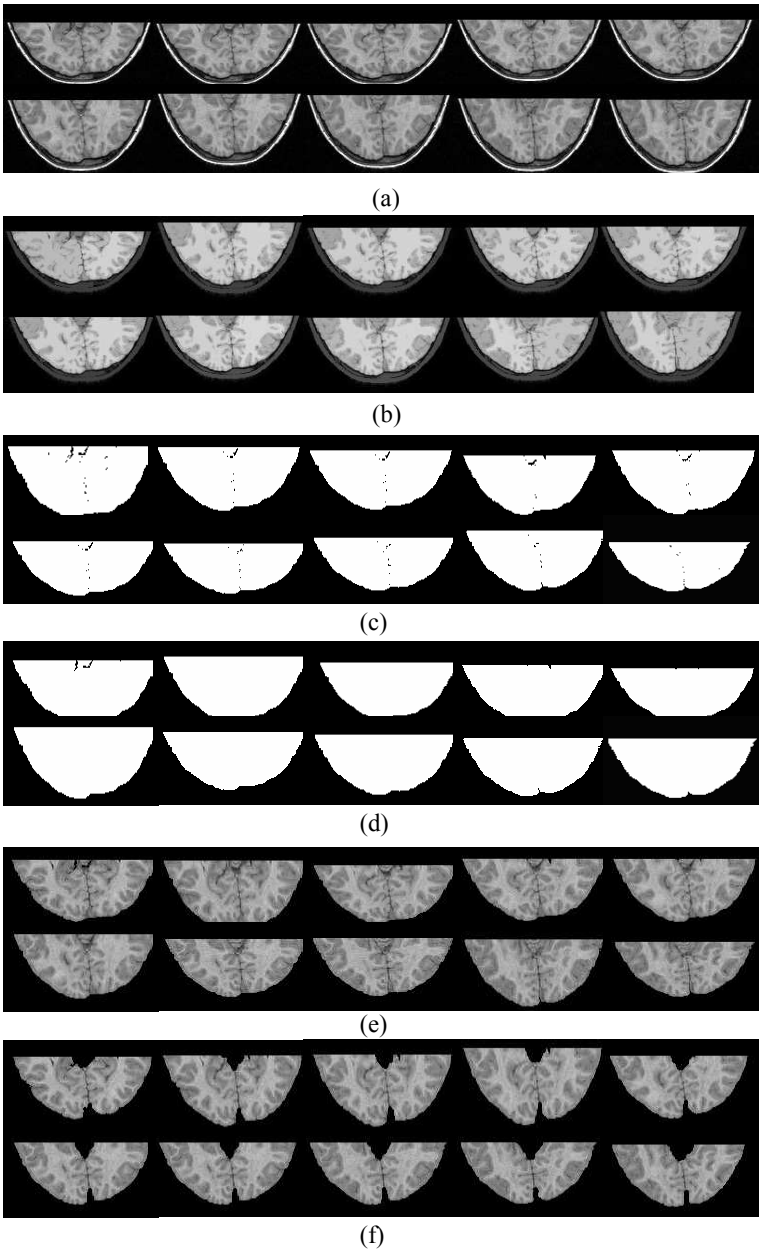

Fig. 6. Images illustrating the procedure followed for skull elimination. (a) Cropped images taken from SSAV1; (b) Opening by reconstruction; (c) Threshold; (d) Closing by reconstruction; (e) Mask; (f) Manual elimination.

(a)

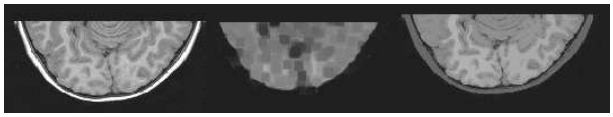

(b)

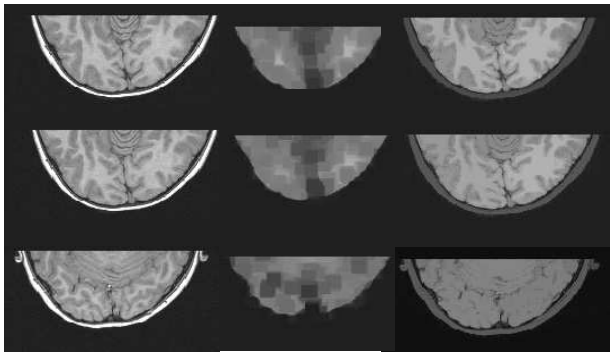

(c)

Fig. 7. Size election of structuring element to attenuate the skull. a) Graph of structures size vs volume on the image $\widetilde{\gamma}_{\mu} - \widetilde{\gamma}_{\mu+1}$, b) Original image , eroded size 3 and opening by reconstruction size 3; c) Original images, eroded size 6, and opening by reconstruction size 6

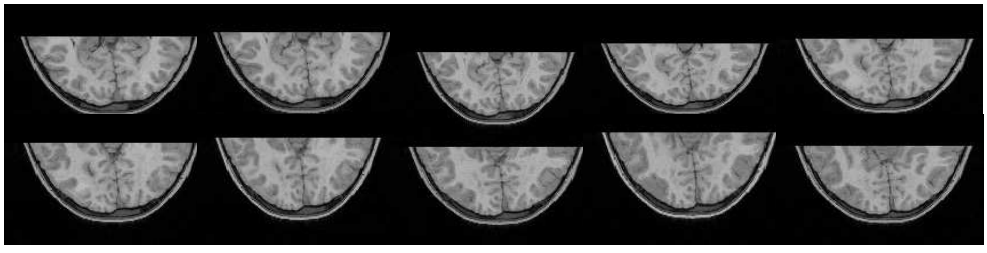

Fig. 8. Opening by reconstruction size $\mu = 1$ applied to images in Fig. 6(a).

Fig. 10, we present the granulometric patterns for the SS and the mean pattern for the CS following the procedure depicted in Fig. 9. Notice that the first two graphs of mean volume correspond to the DHD subjects and CS group; while the last two to the SSAV subjects and CS group.

The granulometric curves in Fig. 10 provide general information for the clear and dark regions detected in the whole deskulling brain. These curves have the disadvantage of being derived from non-autodual transformations, i.e. clear and dark structures are not treated in individual form. As a consequence, it is necessary to separate WM and GM to obtain the granulometric patterns of these regions. In this work, GM and WM were segmented by applying the methodology used in (20). Some output images illustrating the segmentation of such regions are presented in Fig. 11, and the granulometric patterns of WM and GM for the SS and SC are presented in Fig. 12. These graphics were obtained under the procedure depicted in Fig. 9.

4. Results

In particular, we consider three main groups of clear and dark structures. These groups take into account the size of the structuring element (the structuring element used in this paper is a square, see subsection 2.1).

Group 1(Small structures).-In this group the structures within the sizes 1 and 2 of the structuring element are comprised. *Group 2(Medium structures).*- This group contains the structures located in the size interval 3 to 6 of the structuring element. *Group 3(Large structures).*-Finally, this group comprises structure sizes 7-17 of the structuring element.

i) Clear and dark regions analysis from graphics in Fig. 10 for DHD case.-

In both clear and dark regions, a great variation in the curves of DHD subjects is observed with respect to the CS, mainly in medium and large sizes. This indicates the lack of smooth transitions between the analyzed structures.

ii) Clear and dark regions analysis from graphics in Fig. 10 for SSAV case.- Main changes in clear structures are observed in large size structures; while dark structures vary for all sizes.

Curves in Fig. 10 indicate the existence of important variations in clear and dark structures in the DHD and SSAV subjects with respect to the CS. However, clear and dark structures are mixed, and results difficult to infer, since it is not possible to determine whether the predominance or the absence of some structures sizes is due to clear or dark components. This situation occurs because WM and GM have different intensities, and the morphological transformations used to build equations 3 and 4 are not autoduals, i.e, they do not try clear and dark structures in a separate form; this causes that, some clear and dark components are mixed during the processing.

Trying to avoid this inconvenience, WM and GM will be analyzed in separate ways with the purpose of finding some morphometric differences between CS and SS.

iii) WM and GM analysis from graphics in Fig. 12 for DHD case.-

From graphs in Fig. 12, for WM and GM in the SS case, we observe the following: a) a lack of small components with respect to CS; b) the existent small components are thin; and c) medium and large structures predominate in WM and GM.

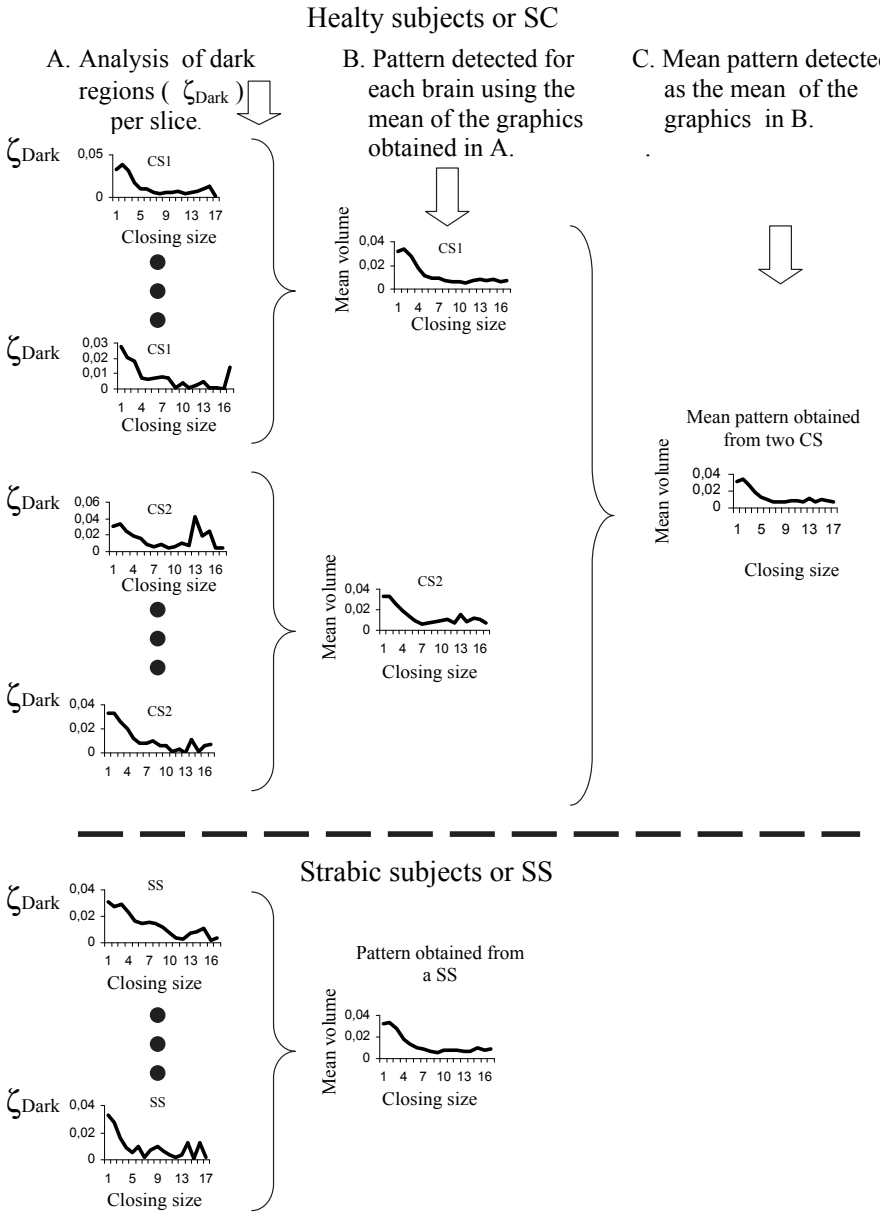

Fig. 9. Procedure to obtain granulometric patterns. In step A the graphics obtained for one slice of each of the two CS and for one SS case are illustrated. In step B, a common mean pattern is obtained for both CS and one SS. Finally, in step C, a mean pattern is obtained for the two CS.

DHD vs CS case:

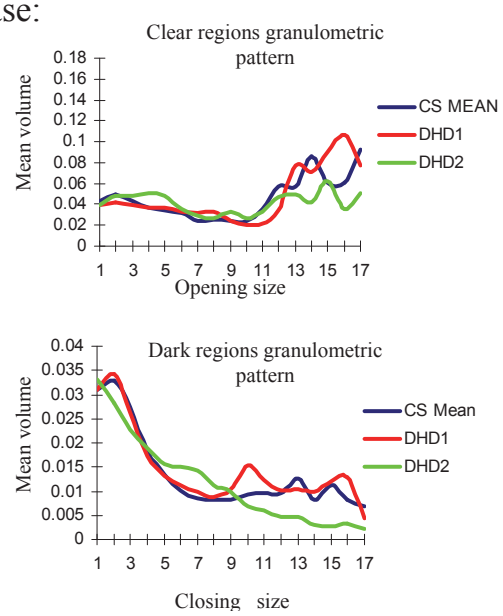

SSAV vs CS case:

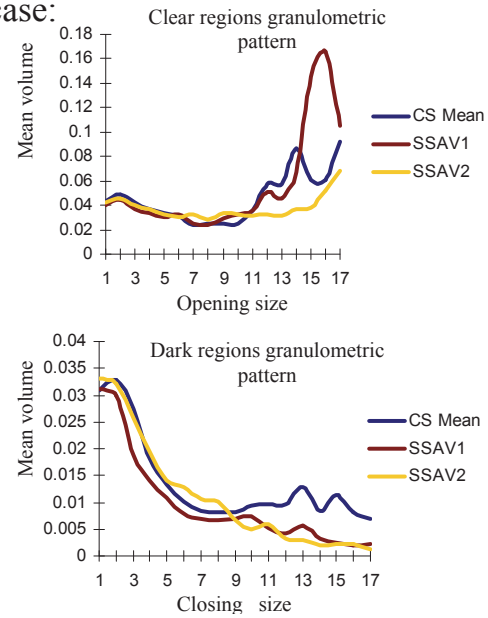

Fig. 10. Mean volume of clear and dark structures corresponding to SS and SC.

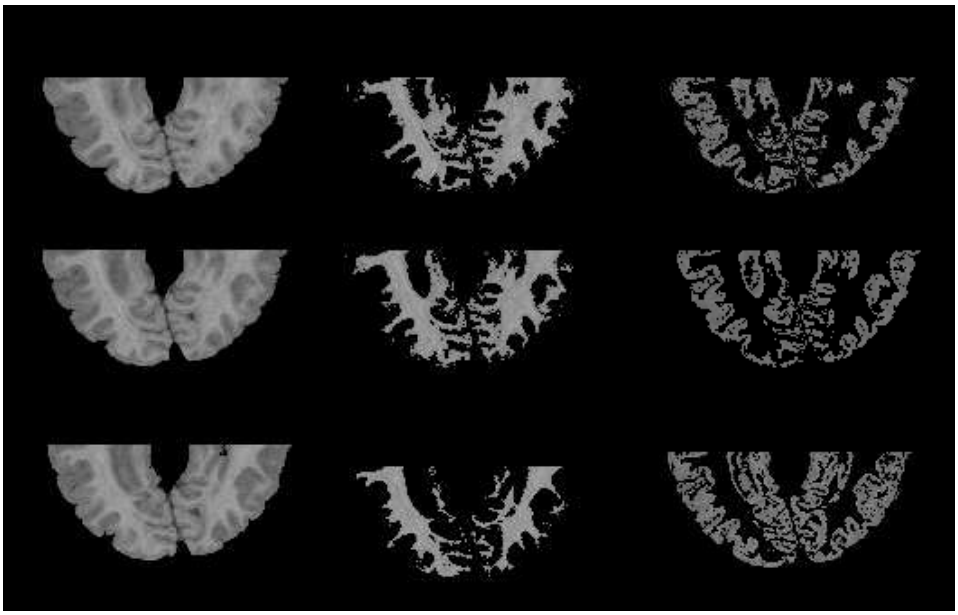

Fig. 11. Images illustrating the segmentation of WM and GM.

In order to explain this situation we divide the analysis of WM and GM as follows :

a) WM analysis.- In Fig. 13, the terms small, medium and large components are exemplified with some structures. Notice that small components in WM have the appearance of ”fingers”, and medium components have a characteristic neck that joins them to large structures.

The lack of small components in the SS with respect to CS group, indicates the absence of such components in the WM. Also, the graphs indicate that the existing small components are thin; therefore they are eliminated easily by small structuring elements. On the other hand, the prevalence of medium and large structures is due to absence the circumvolutions, this originates a non-smooth transition mainly between small and medium components; since medium and large components are not to much different.

In Fig. 14 small components are eliminated from slices that belong to DHD, SSAV and a CS. Notice that for DHD cases, WM has thin ”fingers” which almost disappear after applying an opening of size 1; whereas for the SSAV case, ”fingers” are not so thin and many of them remain after the same transformation is applied.

Note that, for the CS case, WM shows abundant appendages and coral forms. Also, observe that transitions between medium and large sizes are smooth; however for the DHD and SSAV cases, the appendages and coral forms decrease significantly.

b) GM analysis.- In the GM there is a prevalence of medium and large components. This is confirmed in the graphs of GM for DHD and SSAV cases (Fig. 12). Small, medium and large size components in GM are illustrated in Fig. 13.

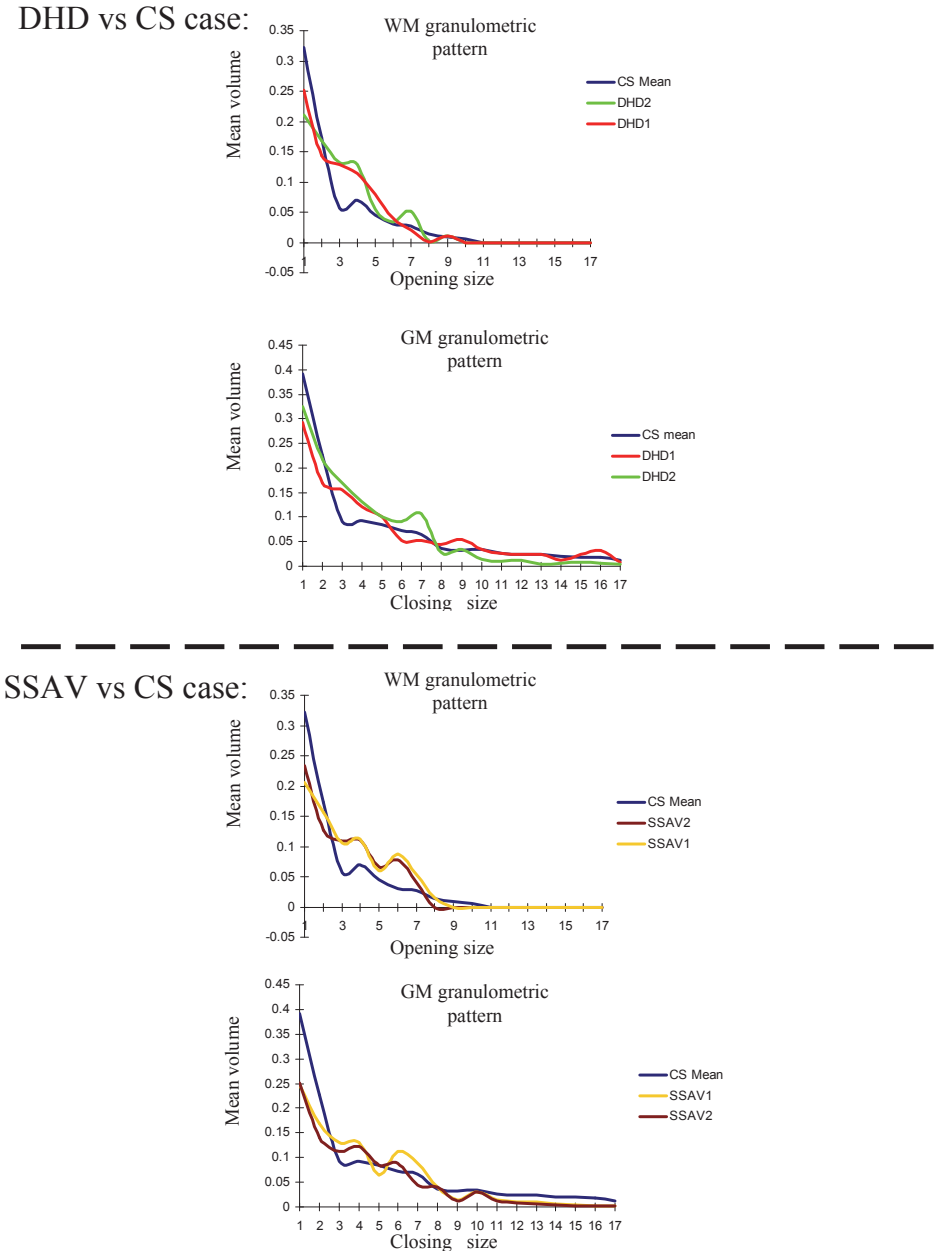

Fig. 12. WM and GM granulometric patterns for the CS and SS groups.

In trying to obtain a parameter indicating the absence, thinning, or thickening of WM or GM structures, an index is proposed. Such index is expressed as follows:

$$\iota = \frac{vol(small\ structures)}{vol(medium\ structures) + vol(large\ structures)} \tag{5}$$

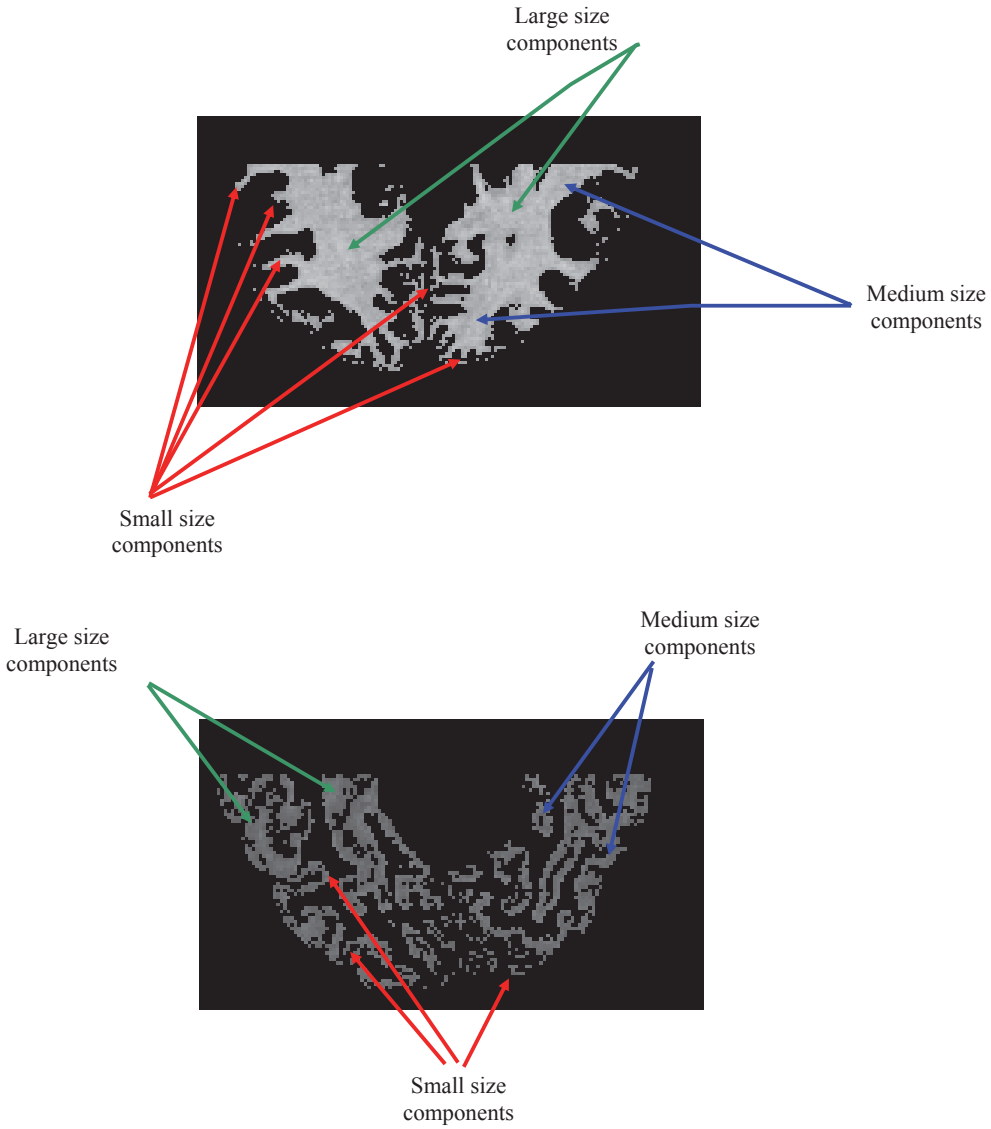

Fig. 13. Illustration of small, medium and large structures on WM and GM.

In Fig. 15, index ι was plotted for WM and GM based on the values obtained for graphs in Fig. 12. When index ι for the CS is compared with that for the SS group, significant differences are obtained, since the latter value is much smaller.

Index ι, indicates that in the WM of CS, the volume of small components is more than double that of medium and large structures together; while in GM of CS, index ι is almost equal to the unit, that is, vol(small structures) $\approx$ vol(medium structures) + vol(large structures).

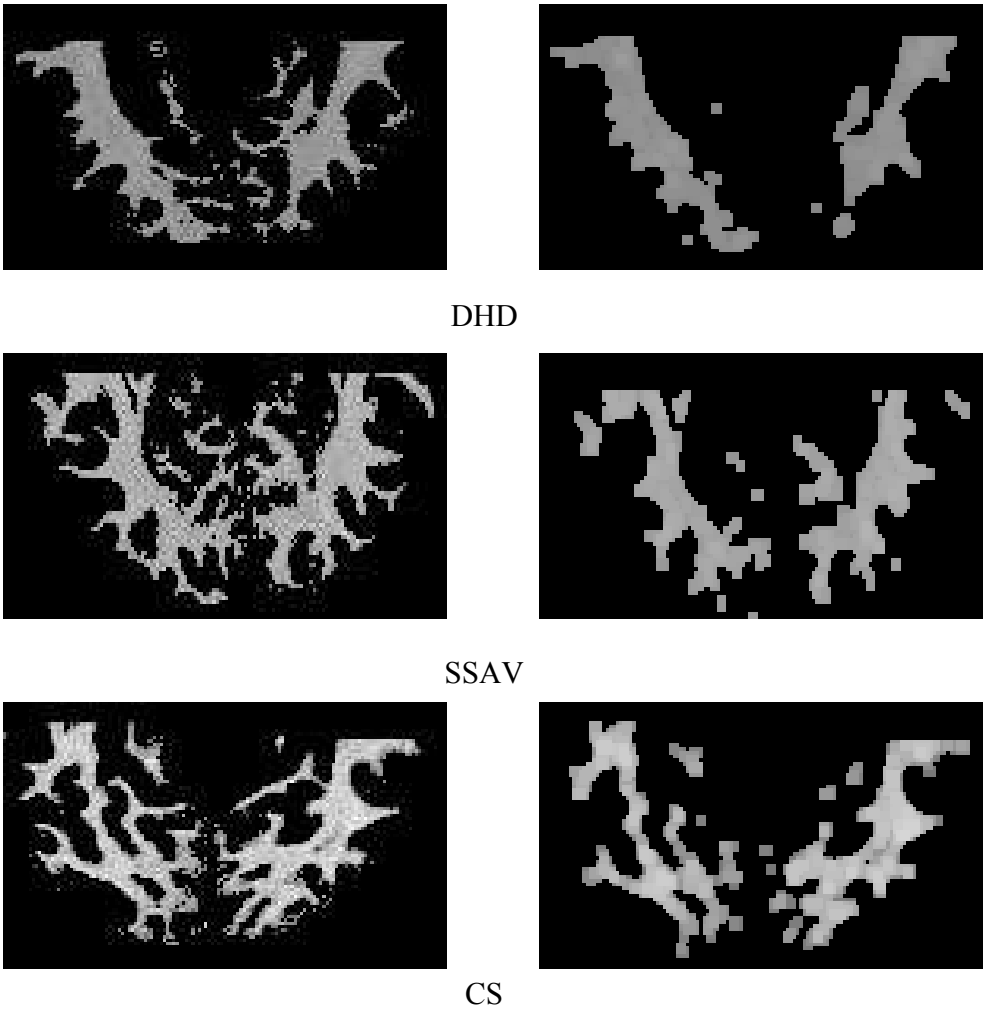

Fig. 14. Elimination of thin components.

With respect to SS, index ι presents the following behavior: a large number of medium components in WM and GM, that yields an inferior value when compared against the index for CS.

In other words, index ι for WM and GM in SS suggests: a) a lack of small components in the analyzed WM, and whenever present they are characterized by their thinness. Medium structures predominate through the analyzed WM. Given the lack of small components, and the presence of thin small structures in WM, this originates the absence of small structures in the GM, for which a predominance of medium and large structures is observed.

The absence of small components (´´fingers") in the WM may causes a lack of electrical connection among different cortical regions. As a consequence a right electrical

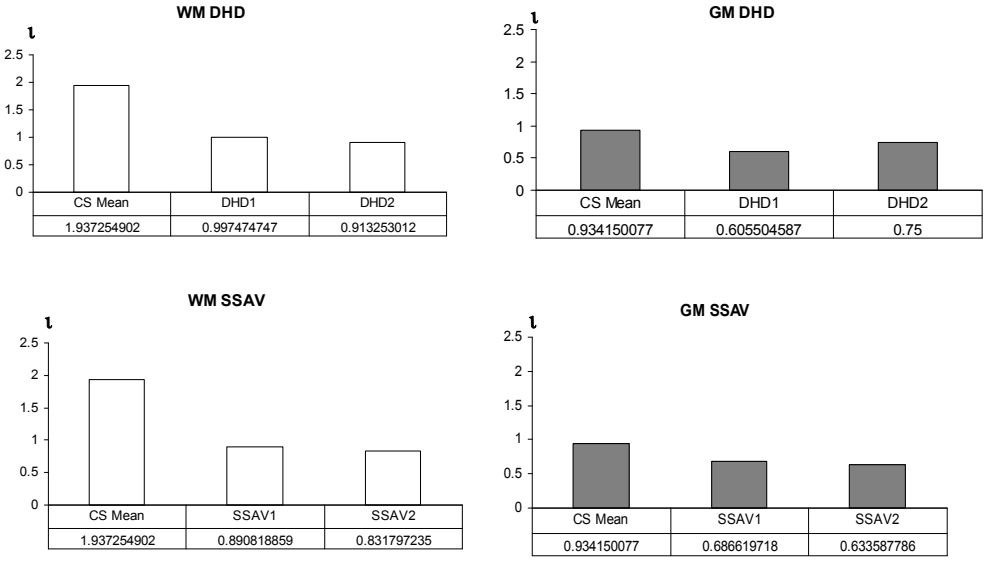

Fig. 15. Table to analyze WM and GM in all subjects through the proposed index ι. Volume values(bottom of x-axis) to evaluate the index were obtained from graphs in Fig. 12.

communication between different cortical areas is hindered. Therefore, although there are great areas of GM and WM in the SS, the lack of small components identified as fingers or thin components in the WM and GM, may cause a faulty electrical conduction and communication between these areas.

On the other side, the presence of a large volume formed of medium components in WM can be associated with a certain immaturity process, which is identified by some authors with excessive glial proliferation or abnormalities in myelin maturation or composition (27). This produces a low quality WM characterized by axons presenting certain degree of damage, with the subsequent deficiency in impulse conduction. In our case, index ι is also called immaturity index, by means of which the absence and increment of certain structures in WM or GM are measured. In this way, morphometric changes in WM and GM seem to be intimately related to the electrical and neurofunctional behavior of the analyzed SS. The granulometric study carried out in this work suggests that changes in the nerve conduction, as we have observed by means of DBM in strabismic patients (7; 8; 14; 15), could be the consequence of changes in the microstructural organization of the cerebral mass. According to this study, these alterations may be manifested as presence of immaturity of certain brain regions and lack of electrical communication between the structures conforming the WM and GM. We consider that as a result of this immaturity, alternative vias are established affecting the processes of neuronal interconnections; with the subsequent affectation, in different degrees and ways of the grey and white substance; hence different clinical expressions of the dissociated strabismus are originated.

On the other hand, studies of electrical brain function carried out by means of computed neurometry, have revealed the close correlation between the structure and cerebral function. This has been determined from the study of electrical coherence, which is a non invasive

method to determine the functional relations among different brain areas. This coherence is altered when some association vias (short and large cortico-corticals, cortico-subcorticals, and short cortico-corticals), are affected structurally; this has been demonstrated in some diseases like Alzheimer's and dementia. Some aspects of the electrical behavior as in the coherence case, depend precisely on the neuro-structural substrate (28; 29). For some authors, a decrease in coherence represents a diagnostic marker. Therefore, further research is necessary on the interrelation between structure and neuronal function, to gain a better understanding into the origin of multiple diseases that have a seat in the cerebral cortex, or at least of those conditions in which the participation of the brain cortex plays a role in their physiopathology. This knowledge enable the establishment of better treatments (28).

On the other hand, during the development of the cerebral cortex or corticogenesis, there is a cellular migration of neurons that travel from periventricular regions and at the same time start maturing, until they reach more superficial regions of the brain, where their maturation culminates. During this process, interconnection vias are liable to be damaged giving place to different neurological schemes, that can affect the neuronal maturity process as well as the performance of the association routes. In the case of strabismus it is still not known, which structural alterations are the cause of this condition. (30–32). Finally, the granulometric study presented in this work, helps us understand the morphology of WM and GM at macroestructural level; however further studies are necessary to analyze the structure of the WM and GM at microestructural level.

5. Conclusions

In this work we presented a method for segmenting MRI slices, as well as the computation of two granulometric studies. The first granulometric study, analyzes clear and dark structures in the whole deskulling brain; while the second one, consists in the analysis of WM and GM separately.

Curves obtained for the whole deskulled brains were not appropriated for analyzing clear and dark regions, since WM and GM are partly composed by pixels of similar intensities.

On the other hand, important differences were found in the granulometric plots of WM and GM of the SS when compared to the graphs of CS group. Main differences consist in the lack of small components ("fingers") and predominance of medium and large structures. From this analysis, index ι was introduced, which is useful to establish an immaturity degree. In the SS, index ι results to be much smaller than that of CS; given the presence of numerous medium and large structures.

The information drawn from these results suggests that there is a faulty electrical communication among several cortical areas due to the lack of small components, and also to the thinness of these structures which are present both in WM and GM. Changes in nerve neuroconduction, similar to those observed by means of the DBM in strabismic patients (7; 8; 14; 15), could be related to the microstructural organization of the cerebral mass. Index ι values, obtained in this work from healthy and strabismic children, show significant differences in the proportion of granulometric elements in the GM and WM when healthy and SS are compared. Based on the calculated index, strabismic patients with SSAV present a

greater degree of immaturity than those patients with DHD; since ι index is smaller. This can be more clearly appreciated from the graphs and derived values in Fig. 15.

On the other hand, it is rather convenient that changes consistent with the alterations in the relation volume and granulometric density can be determined in alive subjects; besides this advantage can be complemented with neurofunctional studies such as the DBM. This technique offers a high temporary resolution, though its space resolution is significantly slower. Granulometric studies offer a finest structural analysis available in vivo, that allow the interpretation of neurofunctional studies. On the one hand, granulometry is outlined as an excellent diagnosis marker for several neurologic diseases. The study carried out in this work not only suggests the neuronal immaturity associated with strabismus, but also the lack of small components("fingers") and the predominance of medium size structures mainly in the SS group. These circumstances propitiate alterations in conduction of the neuroelectrical impulses, favoring the presence of strabismus, as well as the alterations encountered in the DBM. Therefore, granulometric studies may help to gain a better insight into the origin, diagnosis and prognosis of this prevalent disease, for which so little is known. Although the amount of brains analyzed here is only six, they provide important information to establish granulometric differences between SC and SS groups. Finally, for our future research, we are considering the following things: I) Improvement of the morphologic operators involved in the obtention of granulometric curves; these operators must be autodual with the purpose of treating clear and dark components of the image separately; and II) Inclusion of a larger sample of healthy children to obtain mean patterns, as well as a larger number of patients with strabismus.

6. Acknowledgements

The authors wish to thank the Mario Moreno Reyes foundation for the financial support. Jorge D. Mendiola-Santibañez thanks to CONACyT for the financial support.

7. References

[1] Krachmer JH, Marti T.J, Corbett JJ.: Trastornos del quiasma y de las vías visuales retroquiasmáticas, En: Los requisitos en oftalmología: Neuroftalmología. Ed. Harcourt, Madrid, España. 2001; 101-108.

[2] Rakic, P; Lombroso, P.J. "Development of the cerebral cortex: I. Forming the cortical structure". J. Am Acad Child Adolesc Psychiatry 1998, 37 (1): 116-117.

[3] Zeki, SM., Watson, J.D.G, Lueck, C.J., Fristcn, K.J., Kennard, C. And Frackowiat, S.J. "A direct demostration of functional specialization in human visual cortex". J Neurosci 1991, 11(3) 641-649.

[4] Mendola JD, Conner IP, Anjali R, Chan ST, Schwartz TL, Odom JV, Kwong KK. "Voxel-based analysis of MRI detects abnormal visual cortex in children and adults with amblyopia". Human Brain Mapping 2005; 25(2) 222-236

[5] Suk-tak Ch; Kwok-win T; Kwok-cheung L; Lap-kong Ch; Mendola JD; Kwong KK. Neuroanatomy and adult strabismus: a voxel-based morphometric analisys of magnetic resonance structural scans. Neuroimage 2004 (22) 986-994.

[6] Gallegos-Duarte M. "Exploratory maneuvers in congenital endotropy ". En: Temas Selectos de Estrabismo. Centro Mexicano de Estrabismo SC. México, Composición Editorial Láser. México, D.F. 2005, 1-18.
[7] Gallegos-Duarte M; Moguel, S.; Rubín de Celis, B.; " Alterations in the cerebral mapping in the variable congenital endotropy ", Rev Mex Oftalmol; 2004; 78 (3): 122-126.
[8] Gallegos-Duarte M. " Paradoxical cortical response during the intermittent fotoestimulation in the dissociated strabismus ", Cir y Cir 2005; 73 (3): 161-165.
[9] Gallegos-Duarte M, Mendiola-Santibáñez JD, Ortiz-Retana JJ; Rubín de Celis B, Vidal-Pineda R, Sigala-Zamora. " Dissociated desviation. An strabismus of cortical origin". Cir y Cir 2007, 75 (4): (in printt).
[10] Olivares, R; Godoy,G; Adaro,L; Aboitiz, F.: "Neuronal density of the visual cortex (area 17) of two species of wild rodents". Int. J. Morphol 2004, 22 (4): 279-284.
[11] Horton, J.C., Hocking, D.R., "An adult-like pattern of ocular dominance columns in striate cortex of newborn monkeys prior to visual experience". J. Neuroscience 1996, 16:1789-1805.
[12] Horton, J.C., Hocking, D.R., Timing of the critical period for plasticity of ocular dominance columns in macaque striate cortex. J. Neuroscience 1997; 17:3684-3709,.
[13] Tychsen L; Wong AM; Burkhalter A.: Paucity of horizontal connections for binocular vision in V1 of naturally strabismic macaques: Cytochrome oxidase compartment specificity. J Com Neurol. 2004, 474 (2): 261-75
[14] Gallegos-Duarte, M, Moguel-Ancheita S: "Modifications neurologiques adaptatives après traitement médical et chirurgical du syndrome strabique avec variations des repères angulaires". En: Réunion de printemps, Association française de strabologie. 110 Congres de la société Française d´Ophtalmologie, Paris 2004. http://perso.orange.fr/hoc.lods/demo147.html.
[15] Moguel-Ancheita S, Orozco-Gómez L, Gallegos-Duarte M, Alvarado I, Montes C. " Metabolic changes in the cerebral cortex related to the strabismus treatment. Preliminary results with SPECT". Cir y Cir 2004; 72:165-170
[16] Serra, J.: Mathematical Morphology vol. I, Academic Press., London, (1982).
[17] Serra, J. y P. Salembier. "Connected operators and pyramids" ., Proc. of SPIE. Image Algebra and Mathematical Morphology'93, San Diego, July , 1993.
[18] Salembier P., and Serra J.,: Flat zones filtering, connected operators and filters by reconstruction. IEEE Transactions on Image Processing, 3(8), (1995) 1153-1160.
[19] Vincent L. and Dougherty E. R.:Morphological segmentation for textures and particles. In Digital IMage Processing Methods E.R. Dougherty, editor, . Marcel Dekker, New York, (1994) 43–102.
[20] Mendiola-Santibañez, J.D ,Terol-Villalobos, I.R., Herrera-Ruiz G. , Fernández-Bouzas, A., "Morphological contrast measure and contrast enhancement: One application to the segmentation of brain MRI", *Signal Processing*, vol. 87 , no. 9, pp. 2125-2150, 2007.
[21] Soille, P.,: Morphological image analysis: principle and applications, Springer-Verlag, 2003.
[22] Heijmans H., "Morphological Image Operators", Academic Press, USA, 1994.
[23] L. Vincent, "Morphological Grayscale Reconstruction in Image Analysis: Applications and Efficient Algorithms," *IEEE Transactions on Image Processing*, vol. 2, no. 2, pp. 176-201, Feb. 1993.
[24] Matheron G.: Eléments pour une théorie des milieux poreoux. Mason,Paris(1967).

[25] Terol-Villalobos, I.R.: Morphological Image Enhancement and Segmentation, in Advances in Imaging and Electron Physics, P. W. Hawkes Editor, Academic Press, (2001) 207–273.
[26] Mendiola-Santibañez, J.D and Terol-Villalobos, I. R. : Morphological contrast mappings on partition based on the flat zone notion. Computación y Sistemas, 6 (2002b) 25–37.
[27] M. R. Herbert, D. A. Ziegler, C. K. Deutsch,L. M. O'Brien, N. Lange, A. Bakardjiev, J. Hodgson, K. T. Adrien, S. Steele, N. Makris, D. Kennedy1, G. J. Harris and V. S. Caviness Jr ,"Dissociations of cerebral cortex, subcortical and cerebral white matter volumes in autistic boys", *Brain* , vol. 126, pp. 1182–1192, 2003.
[28] Calderón-González P.L, Parra-Rodriguez M.A., Libre-Rodríguez J.J., Gutiérrez J.V. Análisis espectral de la coherencia cerebral en la enfermedad de Alzheimer. Rev Neurol 2004; 38 (5): 422-427
[29] Dunkin JJ, Leuchter AF, Newton TF, Cook IA. Reduced EEG coherence in dementia: state or trait marker? Biol Psychiatry 1994; 35: 870-9
[30] Papovik E, Haynes, L.W Noradrenergic but not cholinergic innervation of the embryonic cortical neuroepithelium rescues germinal and postmitotic cells in heterochronic cocultures. Brain. Res 2000 (853): 227-235
[31] Chiaki Itami, Fumitaka Kimura, Tomoko Kohono, Masato Mtsuoka, Masumi Ichikawa, Tdaharu Tsumoto et Al. Brain-derived neurotrophic factor-dependen unmasking of "silent" synapses in the developing mouse barrel cortex. Neurosciencie 2003 (22) : 13069-13074.
[32] Goshima Y, Ito T, Sasaki Y, Nakamura F. Semaphorins as signals for cell repulsion and invasion. J Clin investigation 2002 (109): 993-998.

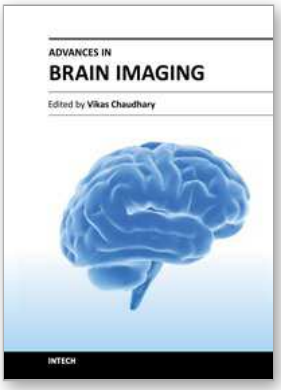

Advances in Brain Imaging

Edited by Dr. Vikas Chaudhary

ISBN 978-953-307-955-4
Hard cover, 264 pages
Publisher InTech
Published online 01, February, 2012
Published in print edition February, 2012

Remarkable advances in medical diagnostic imaging have been made during the past few decades. The development of new imaging techniques and continuous improvements in the display of digital images have opened new horizons in the study of brain anatomy and pathology. The field of brain imaging has now become a fast-moving, demanding and exciting multidisciplinary activity. I hope that this textbook will be useful to students and clinicians in the field of neuroscience, in understanding the fundamentals of advances in brain imaging.

How to reference

In order to correctly reference this scholarly work, feel free to copy and paste the following:

Jorge D. Mendiola-Santibañez, Martín Gallegos-Duarte, Domingo J. Gómez-Meléndez and Angélica R. Jiménez-Sánchez (2012). Comparison of Granulometric Studies of Brain Slices from Normal and Dissociated Strabismus Subjects Through Morphological Transformations, Advances in Brain Imaging, Dr. Vikas Chaudhary (Ed.), ISBN: 978-953-307-955-4, InTech, Available from: http://www.intechopen.com/books/advances-in-brain-imaging/comparison-of-granulometric-studies-of-brain-slices-from-normal-and-dissociated-strabismus-subjects-

INTECH
open science | open minds

InTech Europe
University Campus STeP Ri
Slavka Krautzeka 83/A
51000 Rijeka, Croatia
Phone: +385 (51) 770 447
Fax: +385 (51) 686 166
www.intechopen.com

InTech China
Unit 405, Office Block, Hotel Equatorial Shanghai
No.65, Yan An Road (West), Shanghai, 200040, China
中国上海市延安西路65号上海国际贵都大饭店办公楼405单元
Phone: +86-21-62489820
Fax: +86-21-62489821